Appl. Phys. B 78, 769–774 (2004)
DOI: 10.1007/s00340-004-1503-9

Applied Physics B
Lasers and Optics

L. ZHAO[1,3]
X. WANG[1]
B. WANG[3]
W. WEN[2]
T.-Y. ZHANG[1,✉]

ZnO-doped $LiNbO_3$ single crystals studied by X-ray and density measurements

[1] Department of Mechanical Engineering, Hong Kong University of Science and Technology
[2] Department of Physics, Hong Kong University of Science and Technology, Clear Water Bay, Kowloon, Hong Kong, P.R. China
[3] Electro-Optics Research Center, Harbin Institute of Technology, Harbin 150001, P.R. China

Received: 26 November 2003/
Revised version: 23 February 2004
Published online: 7 April 2004 •

ABSTRACT Energy Dispersive X-ray Fluorescence Spectroscopy, X-ray diffraction and density measurements were conducted on undoped and ZnO-doped congruent $LiNbO_3$ single crystals grown by the Czochralski method. Based on the experimental results, an intrinsic defect evolution model was proposed. When ZnO was doped into the congruent LN crystals, the Zn ions replaced first the Li ions and increased the density. Then, the Zn ions simultaneously replaced the Li ions and the antisite Nb_{Li}s until all Nb_{Li} ions were replaced, which increased the density further. After that, the Zn ions substituted Nb ions in the Nb-sublattice sites with the reduction of the Li vacancies as self-compensation and thus reduced the density. When the Li vacancies disappeared completely, the Zn ions substituted simultaneously both Li ions in the Li-sublattice sites and Nb ions in the Nb-sublattice sites. The simultaneous substitution might finally lead to the generation of oxygen vacancies and decreased the density further.

PACS 61.72.-y; 06.30.Dr; 61.10.-i

1 Introduction

When grown from liquid phase, $LiNbO_3$ (LN) crystals usually have the congruent composition of the mole ratio of $Li_2O/Nb_2O_5 = 48.45/51.55$ with a large Li_2O deficiency. To understand the intrinsic defect structure induced by Li_2O deficiency, the oxygen vacancy model [1] was first proposed, which assumed that there was a deficiency in both oxygen and lithium sites with the chemical formula, $[Li_{1-2x}V_{2x}][Nb][O_{3-x}V_x]$, where the square brackets represent the lithium, niobium, and oxygen sublattices, and V denotes vacancies. The oxygen model predicts a decreasing crystal density with increasing Li_2O deficiency, which is opposite to the experimental measurement [2]. That was why the lithium vacancy model was then proposed [2], in which excess niobium atoms occupy the lithium sites with the creation of an appropriate amount of lithium vacancies for charge compensation and thus the chemical formula is $[Li_{1-5x}Nb_xV_{4x}][Nb][O_3]$. The lithium vacancy model is widely accepted because it is supported by most experimental results and theoretical analysis [3–6]. In the present work, we shall start our analysis with the lithium vacancy model.

To improve the material properties, various dopants have been introduced into the LN crystallographic frame, thereby resulting in the attractive versatility for industrial applications [7]. Among the various dopants Mg and Zn ions behave similarly in many aspects because both are bivalent. For examples, Mg or Zn addition into LN enhances the optical damage-resistance two orders in magnitude and there is a threshold of the Mg or Zn concentration, beyond which the optical damage-resistance jumps 100 times [8–10]. The thresholds are respectively about 5 mol % for MgO and 6.0 mol % for ZnO in the congruent melt [9, 11]. The mole percentage at the congruent melt may be called the nominal concentration because the real concentration may deviate from it. However, as with undoped LN, a dark trace is also induced in Mg-doped LN by the high laser beam [12]. Therefore, Volk et al. [13] suggested the use of ZnO-doped LN that did not exhibit the darkening effect under a laser beam with up to 120 MW/cm^2 in intensity. Di Paolo et al. [7] also found that the Zn diffusion is an effective technique for the fabrication of waveguide lasers, avoiding photorefractive damage and allowing the design of active devices in LN substrates. Espeso–Gil et al. [14] characterized surface layers in Zn-diffused LN waveguides, showing that Zn ions might substitute Li ions. The congruent LN crystals with high ZnO doping are also promising candidates for making low field poled quasiphase-matching structures [15].

Volk et al. [11] studied the properties of damage-resistant LN crystals doped with Mg, Zn or In. They believed that the improvement of damage resistance is due to an essential increase in the photoconductivity and the increase is directly related to the reduction of the intrinsic defects of antisite Nb_{Li} because of the substitution of the doping atoms of Mg, Zn or In. Furthermore, the high photoconductivity of ZnO doped LN leads to a high speed in hologram recording [16]. Volk et al. [17] studied the intrinsic defect structure of ZnO doped LN crystals by using precise X-ray diffraction methods. The value of the real Zn concentration in the ZnO doped LN crystals, [Zn], is calculated from $[Zn] = 1.649[Zn]_m - 0.082[Zn]_m^2$, where $[Zn]_m$ is the nominal con-

✉ Fax: +852-2358-543, E-mail: mezhangt@ust.hk

centration at melt [18]. According to the experimental results from the precise X-ray diffraction on the single crystals and powders, Volk et al. [17] proposed the following chemical formulas

$$[Li_{1-5x}Nb_xV_{4x}][Nb][O_3] \quad (1)$$

for undoped LN,

$$[Li_{1-5x-2y}Nb_xZn_yV_{4x+y}][Nb][O_3] \quad (2)$$

for doped LN with $0 < [Zn] < 5$ mol %,

$$[Li_{1-2x}Zn_xV_x][Nb][O_3] \quad (3)$$

for doped LN with 5 mol % $< [Zn]$,

$$[Li_{1-3y}Zn_{3y}][Nb_{1-y}Zn_y][O_3] \quad (4)$$

for doped LN with $[Zn] > 7$ mol %.

To test the (4) formula, Sulyanov et al. [19] used a compromised formula,

$$[Li_{1-3y-5x}Zn_{3y}Nb_xV_{4x}][Nb_{1-y}Zn_y][O_3] \quad (5)$$

for doped LN with $[Zn] > 7$ mol %,

which allowed both residual Nb ions on the Li sites and Zn ions on both the Li and Nb sites. Through neutron and X-ray study of 8.2 at. % Zn doped LN crystals, Sulyanov et al. [19] found that Zn ions occupied both Li and Nb sites, and there was no residual Nb ions on the Li sites, thereby verifying (4). For $[Zn] = 7.6$ mol %, however, Volk et al. [17] used the formula, $[Li_{0.939}Zn_{0.06}V_{0.001}][Nb_{0.98}Zn_{0.015}V_{0.005}][O_3]$, in their analysis because their experimental results indicate that vacancies exist in both Li and Nb sites.

Using X-ray diffraction on powder samples, Abdi et al. [20] measured the change in lattice constants of ZnO doped LN single crystals as a function of the Zn concentration that was estimated from the same equation as used by Volk et al. [17]. Zhang et al. [9] also conducted X-ray powder analyses and observed similar changes in the lattice parameters as those reported by Abdi et al. [20]. The lattice constants were given by Zhang et al. [9] as a function of the nominal Zn concentration at melt. We may convert the nominal Zn concentration at melt to the Zn concentration by the same formula used by Volk et al. [17] and then compare Zhang et al.′s results [9] with Abdi et al.′s [20], which is shown in Fig. 3 and will be discussed later. However, the experimental results by Kim et al. [21], who determined the lattice constants by the least square method of X-ray diffraction, show an opposite trend. Furthermore, Kim et al. [21] found that the *a*- and *c*-lattice parameters were 0.53316 nm and 1.35887 nm, respectively, for the nominal Zn concentration of 9 mol %. They attributed the abnormal change in the lattice constants to the formation of secondary phase. Nevertheless, the experimental results do indicate that the lattice volume changes with the dopant concentration, which may play a crucial role in density calculations. Comparison of calculated density with measured density is a widely used method to explore the intrinsic defect structure of doped LN crystals. We shall employ the density method to study the intrinsic defect structure of Zn-doped LN crystals. In addition to the direct measurement of the lattice constants, we directly measure the Zn concentration by energy dispersive X-ray fluorescence spectroscopy.

2 Experiments

A series of Zn doped LN single crystals were grown along the *c* axis in air from the melt of the congruent composition using the conventional Czochralski method. The starting materials were prepared by mixing a designed amount of ZnO powders with the powders of Li_2CO_3 and Nb_2O_5 at the mole congruent ratio of $[Li]/[Nb] = 0.946$ for 24 hours. The concentrations of ZnO powders were 4, 6, 8, 10 mol %, respectively. All raw materials were of 99.99% purity. After mixing, the powders were put into a 50 mm high platinum crucible with a 50 mm diameter, and heated to 700 °C for 2 h to decompose the carbonate, then to 1150 °C for 2 h to have the ZnO doped LN polycrystalline materials. The crystals were grown from the polycrystalline materials in diameter-controlled Czochralski equipment with a SiC heater furnace. The temperature gradient along the *c* axis was set as 40 °C/cm and the growth rotation rate was 20 rpm, thereby yielding a growth rate of 2.5 mm/h. About 80% of the melt was crystallized to produce a 20 mm long crystal with a diameter of 20 mm. After growth, the crystal was cooled down to room temperature in air at a cooling rate of 150 °C/h. Then, the crystal was poled at 1180 °C by conducting a dc current with a current density of 5 mA/cm^2 for 30 minutes. After poling, the crystal was cooled down to 800 °C at a cooling rate of 30–40 °C/h and then to room temperature at a cooling rate of 80–90 °C/h. The crystals were sliced perpendicularly to the *c* axis into about 1 mm thick plates and then to 5 mm × 5 mm × 1 mm samples. The samples were polished on two sides carefully to have good optical quality.

Lattice parameters of undoped and ZnO-doped LN samples were determined at room temperature by powder X-ray diffraction (XRD) (Philips, PW1830). With an agate mortar we manually milled the LN single crystals into powders to prepare samples for the X-ray diffraction.

An energy dispersive X-ray fluorescence spectrometer (EDXFS) (Model JSX-3201Z) with a resolution of 0.05% in detecting Zn and Nb elements was used to determine the exact concentration of ZnO in each LN sample. For a LN crystal doped with a nominal ZnO concentration, we examined three samples taken from three different parts of the single crystal and the measurements were repeated three times on each sample. The accuracy of the measurements of Zn concentration was better than 1%. The averaged values were used in the following analysis.

Densities of the LN samples are determined according to Archimedean principle. The weight measurement was carried out in air and in water by using an electronic balance (METTLER TOLEDO) and the absolute error of the balance was 0.1 mg. Then, the density of a LN sample was calculated from $\varrho = \varrho_{\text{water}} W_{\text{air}}/(W_{\text{air}} - W_{\text{water}})$, where $\varrho_{\text{water}} = 1.00$ g/cm^3 denotes the water density, W_{air} and W_{water} denote the measured weights in air and in water, respectively, and the air density is ignored here.

3 Results and discussion

Figure 1 shows the X-ray diffraction (XRD) patterns for the undoped and doped LN crystals with the zoom-in diffraction patterns of the (006) and (110) peaks. The diffraction patterns exhibit only the LN structure in the crystals for

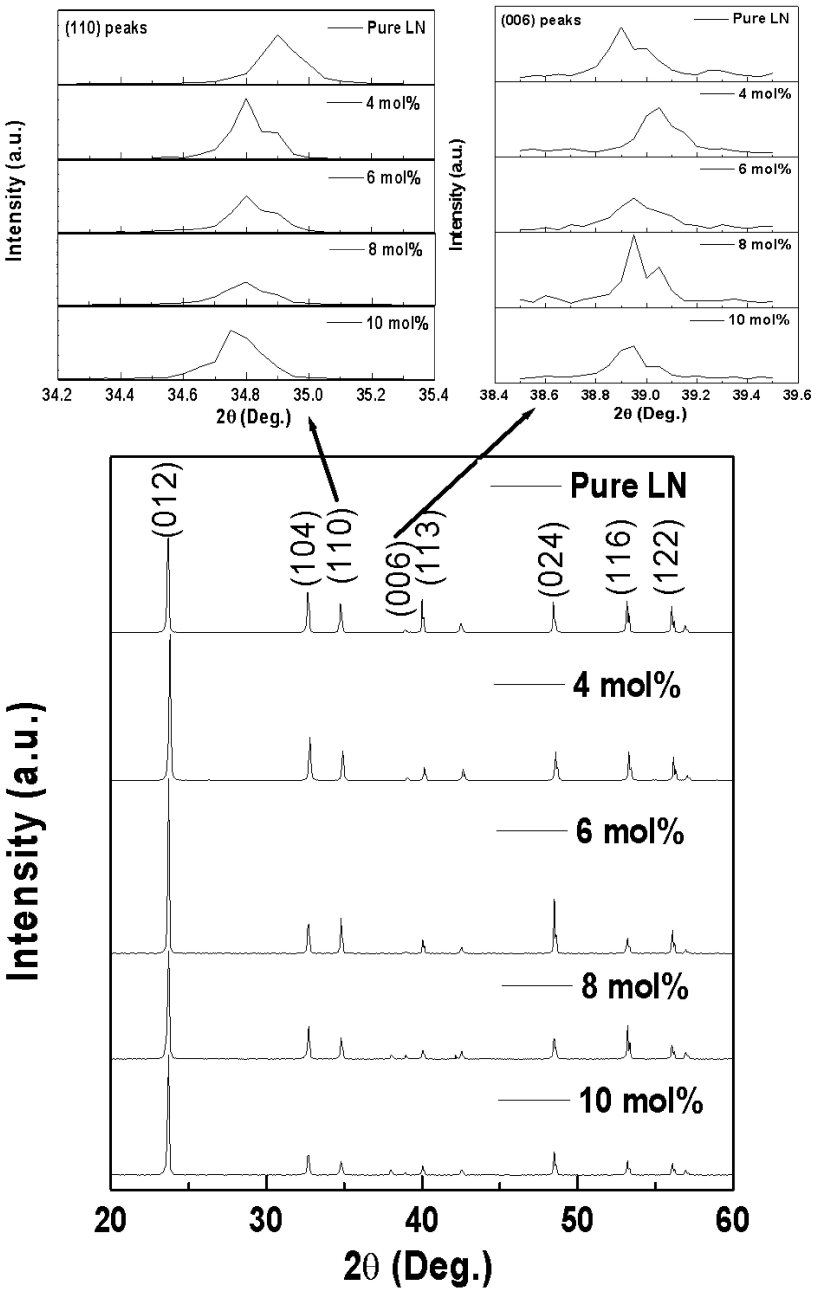

FIGURE 1 X-ray diffraction patterns for the undoped and doped LN crystals with the zoom-in (006) and (110) peaks

all the dopant concentrations, thereby excluding the formation of a secondary phase in the range of the dopant concentrations. After determining the peak positions with the Cohen least square method, we calculated the lattice constants by using the Bragg equation.

Figure 2a illustrates a typical EDXFS result for all the undoped and doped LN crystals. From the EDXFS results, we plot the Zn concentration as a function of the nominal Zn concentration at melt in Fig. 2b. As can be seen in Fig. 2b, the Zn concentrations are correspondingly smaller than the nominal ones. As a comparison, we also plot the calculated Zn concentration from the equation $[\mathrm{Zn}] = 1.649[\mathrm{Zn}]_{\mathrm{m}} - 0.082[\mathrm{Zn}]_{\mathrm{m}}^2$. It seems that the calculated concentrations do not agree with the experimental results. The calculated concentration is higher than the nominal concentration at melt until the nominal concentration of about 7.9 mol %, whereas the measured concentration is always lower than the nominal concentration. The calculated and measured concentrations for the nominal concentration of 4 mol % are respectively 5.28 mol % and 2.16 mol %, yielding a difference of 3.12 mol %.

The XRD and EDXFS results enable us to plot the lattice constants as a function of the Zn concentration. Figure 3a and b show respectively the *a*- and *c*-lattice parameters. For comparison, we also plot the *a*- and *c*-lattice parameters determined by other researchers [9, 20, 21] in Fig. 3a and b. As mentioned above, the Zn concentrations in [9, 20, 21] were estimated from the equation $[\mathrm{Zn}] = 1.649[\mathrm{Zn}]_{\mathrm{m}} - 0.082[\mathrm{Zn}]_{\mathrm{m}}^2$. The present work, as shown in Fig. 3a, indicates that the *a*-lattice parameter increases monotonically, which is consistent with most results of the previous works' expectation of a decrease at 3 mol % Zn in [9] and a decrease at 8 mol % Zn in [21]. On the other hand, we found that the *c*-lattice

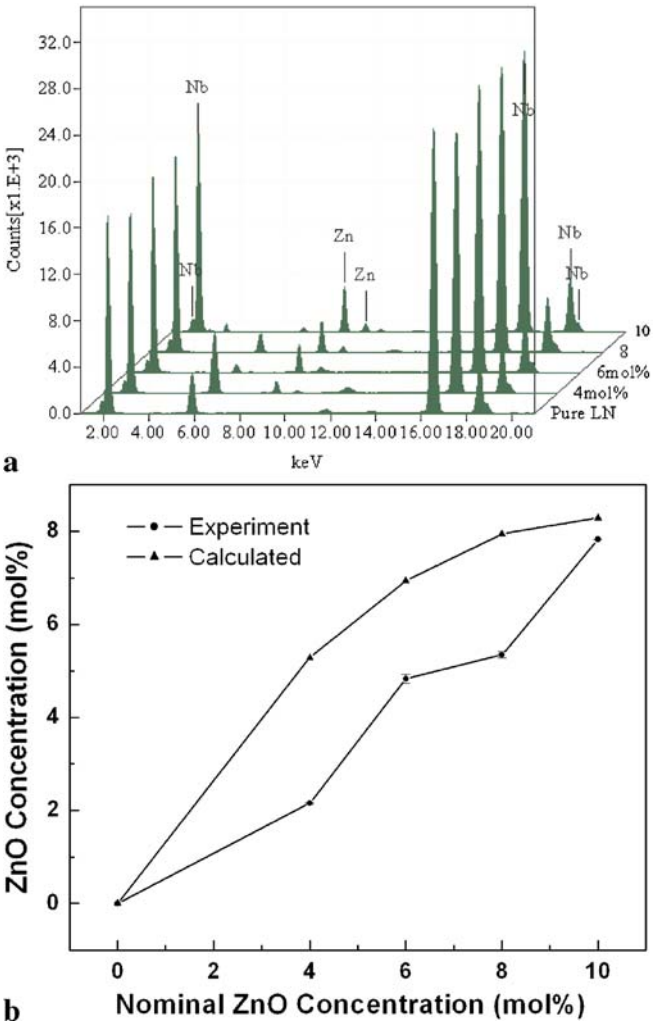

FIGURE 2 **a** Typical EDXFS result for all the undoped and doped LN crystals. **b** The measured and calculated Zn concentration as a function of the nominal Zn concentration at melt

parameter decreases from 1.38625 nm to 1.38562 nm, then increases to 1.38624 nm and almost saturates at 1.38658 nm when the Zn concentration increases from zero to 2.16 mol %, to 4.83 mol % and then to 7.83 mol %. The reduction of the *c*-lattice parameter caused by ZnO doping has been reported in [9, 20]. Figure 3b indicates that the present result is more or less consistent with the results in [9, 20]. The values of the *c*-lattice parameter reported in [21] are much smaller than the corresponding values measured in the present work and those in [9, 20] as well. From the lattice constants we calculate the lattice volume as a function of the Zn concentration and plot the result in Fig. 3c. Figure 3c also illustrates the values of the lattice volume calculated with the data of lattice constants reported in [9, 20, 21]. Clearly, the present result is comparable to the other results [9, 20].

We weighted each sample in air and in water and then calculated its density. Figure 4 shows the variation of the density with the Zn concentration. The density increases from 4.61599 g/cm^3 to 4.71340 g/cm^3 and then reaches a peak value of 4.739454 g/cm^3 when the Zn concentration increases from zero to 2.16 mol % and to 4.83 mol %. After that, further increasing the Zn concentration to 5.35 mol % and 7.83 mol % reduces the density to 4.72535 g/cm^3 and 4.71810 g/cm^3 accordingly.

The measured density and the lattice volume results allow us to explore the intrinsic defect microstructure. We start with the Li-site vacancy model and calculate the undoped LN density with (1), $[Li_{1-5x}Nb_xV_{4x}][Nb][O_3]$. Following Volk et al.′s approach [17], we believe that the doped Zn ions substitute Li ions first. Thus, (2), $[Li_{1-5x-2y}Nb_xZn_yV_{4x+y}][Nb][O_3]$ is adopted to calculate the density of the 2.16 mol % Zn doped LN crystal. Since the atomic weight of a Zn atom, 65.37, is much larger than the atomic weight of two Li atoms, 2×6.939, one Zn atom replacing two Li atoms increases the density. In this case, the occupying ratio of the Li-sublattice sites is smaller than that in the undoped LN crystals. When there are more vacancies in the Li-sublattice sites, the *c*-lattice parameter is reduced and the lattice volume is decreased as well. On the other hand, the atomic size of Zn, 0.074 nm, is bigger than the Li size, 0.068 nm [22], which makes the *a*-lattice parameter larger. Further increasing the Zn concentration will generate more vacancies. When the vacancy concentration is too high, the microstructure becomes thermodynamically unstable and the Zn ions will simultaneously replace Li and antisite Nb_{Li} ions, as proposed by Volk et al. [17]. In the present study, we are not able to determine the critical value of Zn concentration, at which simultaneous replacement of Li and antisite Nb_{Li} ions by Zn ions takes place, due to the lack of experimental and/or theoretical information. Volk et al. [17] did not detect any antisite Nb_{Li} ions at the estimated Zn concentration of 5.2 mol %. Considering that the estimated Zn concentration is lower than the measured one; therefore, it seems to be reasonable to assume that the antisite Nb_{Li} ions disappear at the Zn concentration of 4.83 mol %. Thus, we may use (3), $[Li_{1-2x}Zn_xV_x][Nb][O_3]$, to calculate the density. According to (3), the vacancy concentration is the same as the Zn concentration of 4.83 mol %, while the vacancy concentration is about 5 mol % for the undoped LN crystals. That is why the *c*-lattice parameter in the 4.83 mol % Zn doped LN crystals is more or less the same as that in the undoped LN crystals. When the Zn concentration is higher than a critical value, Volk et al. [17] proposed (4), which indicates that the Zn ions replace Li ions in the Li-sublattice sites and Nb ions in the Nb-sublattice sites and no vacancies will be involved. If considering the transition from (3) to (4), we have to answer how the vacancies in the Li-sublattice sites, as indicated by (3), disappear. We, therefore, propose (6)

$$[Li_{1-2x+3y}Zn_xV_{x-3y}][Nb_{1-y}Zn_y][O_3]. \quad (6)$$

The scenario for (6) is that when exceeding the critical value of 4.83 mol % Zn, the Zn ions replace Nb ions in the Nb-sublattice sites, while the Zn concentration in the Li-sublattice sites remains unchanged at 4.83 mol %. For charge compensation, the vacant Li-sublattice sites are occupied by Li ions. This process continues until the Li-sublattice sites are fully occupied. Since the antisite Nb_{Li} ions disappear at the Zn concentration of 4.83 mol %, (6) is valid from the Zn concentration 4.83 mol % to another critical value at which all the vacancies have disappeared and beyond which (4) describes the defect structure. For clarification, we may rewrite (6) as $[Li_{0.9034+3y}Zn_{0.0483}V_{0.0483-3y}][Nb_{1-y}Zn_y][O_3]$. From the ex-

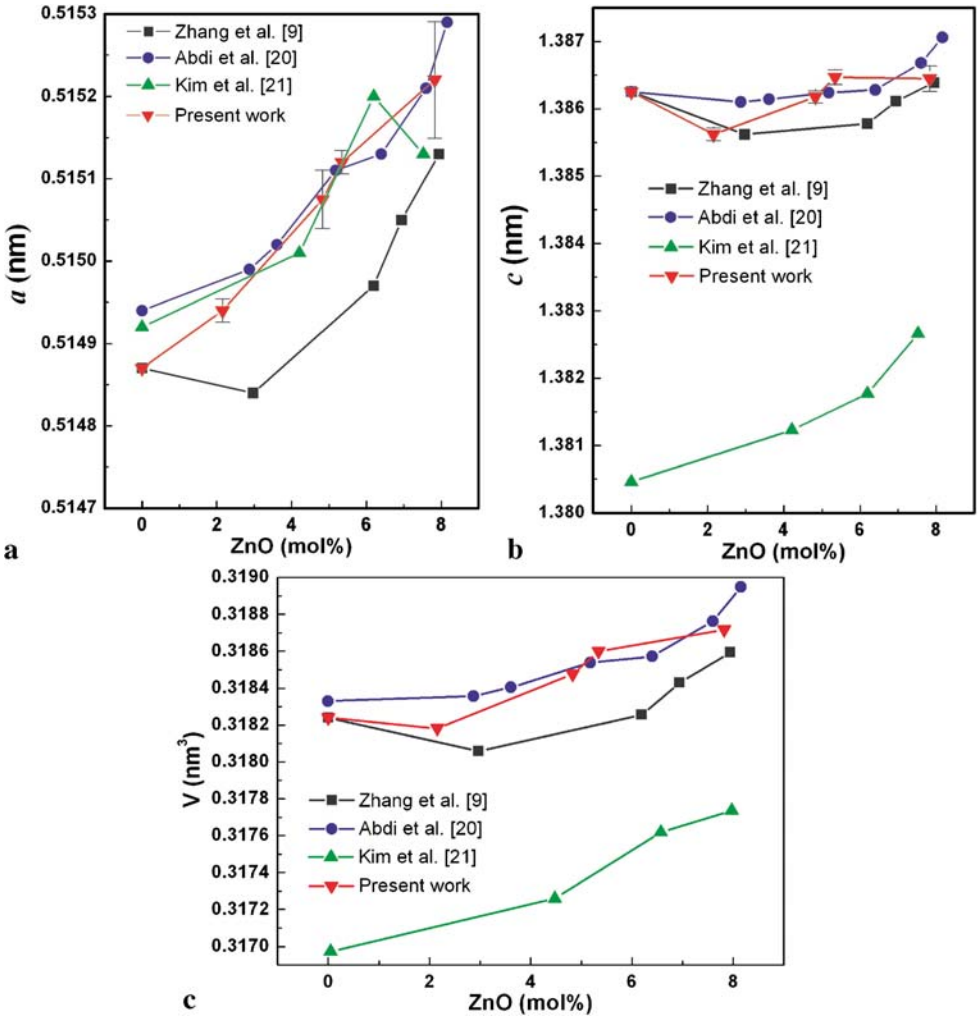

FIGURE 3 **a** The *a*-lattice constant of the Zn-doped LN crystals as a function of the Zn concentration. **b** The *c*-lattice constant of the Zn-doped LN crystals as a function of the Zn concentration. **c** The lattice volume of the Zn-doped LN crystals as a function of the Zn concentration

plicit formula, we have the consequence that no vacancies will exist when $y = 0.0161$, which yields another critical value of the Zn concentration to be 6.44 mol %. At the critical concentration of 6.44 mol %, (6) is reduced to (4). Therefore, for the LN crystals doped with 5.35 mol % Zn, which is between 4.83 mol % (3) and 6.44 mol % (4), we should use (6), $[Li_{0.9189}Zn_{0.0483}V_{0.0327}][Nb_{0.9948}Zn_{0.0052}][O_3]$, to calculate the density. (6) indicates that one Zn atom and three Li atoms are added in as one Nb atom is taken out. Since one Nb atom (atomic weight=92.91) is heavier than the total weight of one Zn atom and three Li atoms, the density of the LN crystals doped with 5.35 mol % Zn is smaller than that doped with 4.83 mol % Zn, which is observed experimentally and shown in Fig. 4. When the vacant Li-sublattice sites are fully occupied, (6) is reduced to (4), thereby describing the transition state from (3) to (4) in the defect evolution.

When the Zn concentration increases further from 5.35 mol %, Volk et al. [17] believed that (4), $[Li_{1-3y}Zn_{3y}][Nb_{1-y}Zn_y][O_3]$, describes the intrinsic defect microstructure. (4) indicates that four Zn atoms are added in as one Nb atom and three Li atoms are taken out. Four Zn atoms are heavier than the total weight of one Nb atom and three Li atoms. Thus, if (4) is used in the calculation of the density of the LN crystals doped with 7.83 mol % Zn, the density will be higher in comparison with the density of the LN crystals doped with 5.35 mol % Zn. However, the opposite trend was observed experimentally, as shown in Fig. 4. To understand the reduction in density, we consider all possible models of intrinsic defects from literature and only an oxygen vacancy

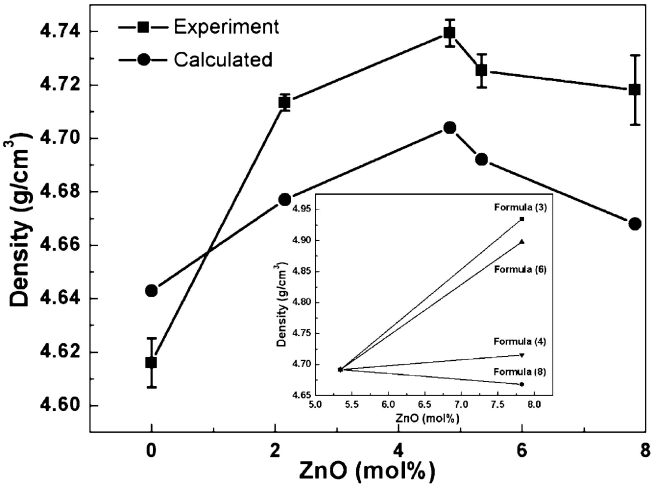

FIGURE 4 The measured and calculated densities of the Zn-doped LN crystals as a function of the Zn concentration, where the inset shows the calculated densities of the LN crystals doped with 7.83 mol % Zn

model can be used to explain the phenomenon. As indicated in (6), all vacant Li-sublattice sites are gradually occupied as the Zn concentration increases. Therefore, in the proposed oxygen model there are no vacancies in the Li-sublattice sites. When two Zn^{+2} ions replace one Li^{+} ion and one Nb^{+5} ion, the following self-compensation is possible:

$$2\,\mathrm{ZnO} + \mathrm{LiNbO_3} \rightarrow [\mathrm{Zn_{Li}}]^{+} + [\mathrm{Zn_{Nb}}]^{-3} + [\mathrm{V}_O]^{+2} + \mathrm{LiNbO_3}. \quad (7)$$

The self-compensation requires a concentration ratio of $[\mathrm{Zn_{Nb}}]^{-3} : [\mathrm{Zn_{Li}}]^{+} = 1 : 1$ and an oxygen vacancy. Thus, (8) should take the form of

$$[\mathrm{Li}_{1-3y-z}\mathrm{Zn}_{3y+z}][\mathrm{Nb}_{1-y-z}\mathrm{Zn}_{y+z}][\mathrm{O}_{3-z}\mathrm{V}_z]. \quad (8)$$

Comparing (8) with (4) implies that the defect microstructure described by (8) may be regarded as an evolution result from the defect microstructure described by (4). With (8), we calculate the density of the LN crystals doped with 7.83 mol % Zn. As expected, the density value is lower than the calculated density of the LN crystals doped with 5.35 mol % Zn. The calculated trend is the same as that observed experimentally, as shown in Fig. 4. The inset of Fig. 4 illustrates the calculated densities of the LN crystals doped with 7.83 mol % Zn by using four formulas. The reduction in the density of highly Zn doped LN crystals cannot be explained by (3), (6), and (4), which all predict an increasing trend in density, except of (8), the oxygen vacancy model.

4 Conclusions

All calculated densities are plotted in Fig. 4 for comparison with the measured results. The absolute values of the calculated densities deviate from the corresponding measured ones with the maximum error less than 1%. Nevertheless, the calculated density, as a function of the Zn concentration, exhibits the same behavior as the measured density. The behavior consistency between the measured and calculated densities supports the scenario of the intrinsic defect microstructure evolution caused by Zn doping. The scenario is basically consistent with that proposed by Volk et al. [17] with the starting from the Li vacancy model. When ZnO is doped into the congruent LN crystals, the Zn ions replace first the Li ions and hence increase the density. Then, the Zn ions simultaneously replace the Li ions and the antisite $\mathrm{Nb_{Li}}$s. The simultaneous replacements of Li and $\mathrm{Nb_{Li}}$ ions continue until all $\mathrm{Nb_{Li}}$ ions are replaced by the Zn ions. It is generally accepted that the resistance to optical damage will jump two orders in magnitude when all $\mathrm{Nb_{Li}}$ ions are replaced [9, 11]. After that, the Zn ions substitute Nb ions in the Nb-sublattice sites with the reduction of the Li vacancies as self-compensation. When the Li vacancies disappear completely, the Zn ions may substitute simultaneously both Li ions in the Li-sublattice sites and Nb ions in the Nb-sublattice sites. The simultaneous substitution might finally lead to the generation of oxygen vacancies. This oxygen model should be further investigated in detail.

ACKNOWLEDGEMENTS This work was supported by an RGC grant from the Hong Kong Research Grants Council, HKSAR, China. The experiments were conducted at the Materials Preparation and Characterization Facility, HKUST. TY Zhang thanks the Croucher Foundation for the Croucher Senior Research Fellowship Award, which gave him more research time by releasing him from teaching duties.

REFERENCES

1 H. Fay, W.J. Alford, H.M. Dess: Appl. Phys. Lett. **12**, 89 (1968)
2 P. Lerner, C. Legras, J.P. Dumas: J. Cryst. Growth **3/4**, 231 (1968)
3 J. Liu, W. Zhang, G. Zhang: Phys. Status. Solidi. A **156**, 285 (1996)
4 B.C. Grabmaier, F. Otto: J. Cryst. Growth **79**, 682 (1986)
5 F.P. Safaryan, R.S. Feigelson, A.M. Petrosyan: J. Appl. Phys. **85**, 8079 (1999)
6 N. Iyi, K. Kitamura, F. Izumi, J.K. Yamamoto, T. Hayashi, H. Asano, X. Kimura: J. Solid State. Chem. **101**, 340 (1992)
7 R.E. Di Paolo, E. Cantelar, P.L. Pernas, G. Lifante, F. Cusso: Appl. Phys. Lett. **79**, 4088 (2001)
8 Y. Furakawa, M. Sato, F. Nitanda, K. Ito: J. Cryst. Growth **99**, 832 (1990)
9 Y. Zhang, Y.H. Xu, M.H. Li, Y.Q. Zhao: J. Cryst. Growth **233**, 537 (2001)
10 D.A. Bryan, R. gerson, H.E. Tomaschke: Appl. Phys. Lett. **44**, 847 (1984)
11 T.R. Volk, N.M. Rubinina, M. Wöhlecke: J. Opt. Soc. Am. B **11**, 1681 (1994)
12 A.M. Glass: Opt. Eng. **17**, 470 (1978)
13 T.R. Volk, V.I. Pryalkin, N.M. Rubinina: Opt. Lett. **15**, 996 (1990)
14 O. Espeso-Gil, G. García, F. Agulló-López, A. Climent-Font, T. Sajavaara, M. Domenech, E. Cantelar, G. Lifante: Appl. Phys. Lett. **81**, 1981 (2002)
15 L.H. Peng, Y.C. Zhang, Y.C. Lin: Appl. Phys. Lett. **78**, 4 (2001)
16 T.R. Volk, N.V. Razumovski, A.V. Mamaev, N.M. Rubinina: J. Opt. Soc. Am. B **13**, 1457 (1996)
17 T.R. Volk, B. Maximov, T. Chernaya, N.M. Rubinina, M. Wöhlecke, V. Simonov: Appl. Phys. B **72**, 647 (2001)
18 U. Schlarb, M. Wöhlecke, B. Gather, A. Reichert, K. Betzler, T.R. Volk, N.M. Rubinina: Opt. Mater. **4**, 791 (1995)
19 S. Sulyanov, B. Maximov, T. Volk, H. Boysen, J. Schneider, N. Rubinina, T. Hansen: Appl. Phys. A **74**, S1031 (2002)
20 F. Abdi, M. Aillerie, M. Fontana, P. Bourson, T.R. Volk, B. Maximov, S. Sulyanov, N.M. Rubinia, M. Wöhlecke: Appl. Phys. B **68**, 795 (1999)
21 K.H. Kim, K.B. Shim, K.H. Auh: Materials Lett. **55**, 116 (2002)
22 W.D. Callister, Jr.: *Materials Science and Engineering, An Introduction* 6th ed. (John Wiley & Sons, Inc., New York 2003)